big data and cognitive computing

MDPI

Article

Suspension Parameter Estimation Method for Heavy-Duty Freight Trains Based on Deep Learning

Changfan Zhang [1], Yuxuan Wang [1] and Jing He [2,*]

[1] College of Railway Transportation, Hunan University of Technology, Zhuzhou 412007, China
[2] College of Electrical and Information Engineering, Hunan University of Technology, Zhuzhou 412007, China
* Correspondence: hejing@hut.edu.cn

Abstract: The suspension parameters of heavy-duty freight trains can deviate from their initial design values due to material aging and performance degradation. While traditional multibody dynamics simulation models are usually designed for fixed working conditions, it is difficult for them to adequately analyze the safety status of the vehicle–line system in actual operation. To address this issue, this research provides a suspension parameter estimation technique based on CNN-GRU. Firstly, a prototype C80 train was utilized to build a simulation model for multibody dynamics. Secondly, six key suspension parameters for wheel–rail force were selected using the Sobol global sensitivity analysis method. Then, a CNN-GRU proxy model was constructed, with the actually measured wheel–rail forces as a reference. By combining this approach with NSGA-II (Non-dominated Sorting Genetic Algorithm II), the key suspension parameters were calculated. Finally, the estimated parameter values were applied into the vehicle–line coupled multibody dynamical model and validated. The results show that, with the corrected dynamical model, the relative errors of the simulated wheel–rail force are reduced from 9.28%, 6.24% and 18.11% to 7%, 4.52% and 10.44%, corresponding to straight, curve, and long and steep uphill conditions, respectively. The wheel–rail force simulation's precision is increased, indicating that the proposed method is effective in estimating the suspension parameters for heavy-duty freight trains.

Citation: Zhang, C.; Wang, Y.; He, J. Suspension Parameter Estimation Method for Heavy-Duty Freight Trains Based on Deep Learning. *Big Data Cogn. Comput.* **2024**, *8*, 181. https://doi.org/10.3390/bdcc8120181

Academic Editors: Hongshan Yu, Zhengeng Yang, Mingtao Feng and Qieshi Zhang

Received: 13 October 2024
Revised: 20 November 2024
Accepted: 2 December 2024
Published: 4 December 2024

Keywords: deep learning; heavy-duty freight trains; machine learning; CNN-GRU model; parameter estimation

1. Introduction

As demand for the transportation of heavy-duty freight trains increases, trains are operating with higher loads under complex and changing line conditions. The effectiveness and safety of the overall transportation system are closely correlated with the operational safety and stability of trains [1,2]. The suspension system is the core structural component supporting the stable running of heavy-duty freight trains. Therefore, the design and adjustment of its parameters are particularly important. However, during long service, the parameters of suspension systems for heavy-duty freight trains can deviate from their initial design values due to material aging and performance degradation, resulting in a decrease in vehicle dynamics performance [3,4]. As traditional multibody dynamics simulation models are usually designed for fixed working conditions, it is difficult for them to fully and accurately assess the status of the vehicle–line system. For this reason, it is crucial to use advanced machine learning techniques and data-driven methods to estimate and optimize suspension parameters.

In the field of track–vehicle system identification and parameter estimation, the research can be broadly classified into two directions, i.e., numerical estimation methods based on

track–vehicle dynamics simulation modeling [5,6] and methods based on machine learning [7–9]. Among them, as one of the machine learning methods [10,11], the proxy model, combined with a deep learning model, can effectively capture comprehensive dynamic characteristics of trains during operation, simplify the original complex model and derive accurate results faster, such that the safety and reliability of the transportation system can be improved. Mohamed et al. [12] sought to optimize a passive vehicle suspension system by using the HHO (Harris Hawk Optimization) algorithm. Qing et al. [13] discussed an approximate Bayesian method to accurately estimate the suspension characteristics of high-speed trains in operation. Zou [14] used a surrogate model to replace the high-precision dynamical model, for the purpose of developing a quick optimization technique for suspension parameters under various circumstances. Pan et al. [15] comprehensively studied various machine learning methods in the field of estimating suspension parameters.

To achieve the accurate estimation of suspension parameters for heavy-duty freight trains, this paper utilizes actual values of wheel–rail force measurements from heavy-duty freight trains, constructs a proxy model based on CNN-GRU, and combines sensitivity analysis and an optimization algorithm. Figure 1 depicts the overall procedure, and the primary contributions of the method are as follows:

(1) A database of wheel–track interaction force values recorded by the force measuring system is established, including wheel–track interaction force data under three typical working conditions, i.e., straight, curve, and long and heavy uphill conditions. This provides reliable data for the training of the proxy model;
(2) A suspension parameter estimation method is proposed. It is data-driven and based on the mechanism model. Using a proxy model and an optimization algorithm, it estimates the suspension parameters, providing a new approach to accurately evaluate the safety state of heavy-duty freight trains;
(3) The proposed method's usefulness is demonstrated through comparative trials, resulting in a new approach for ensuring vehicle safety and stability.

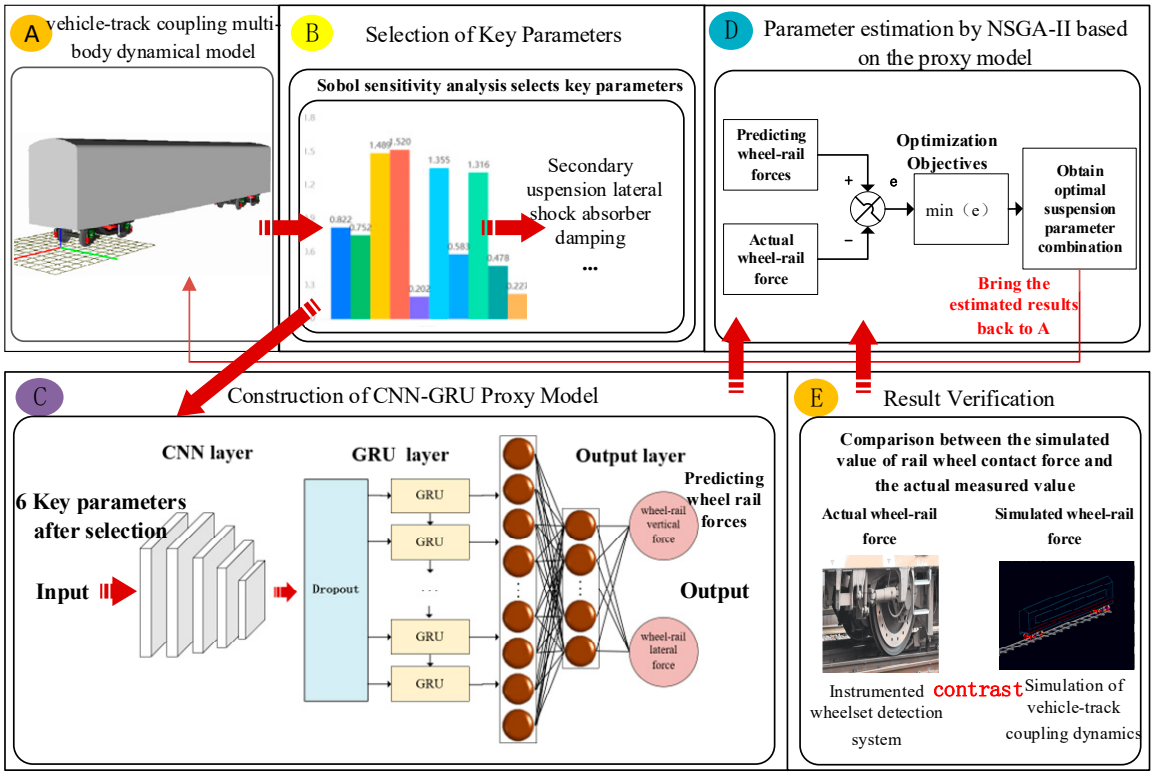

Figure 1. Overall block diagram of CNN-GRU parameter estimation algorithm.

2. Establishment of a Multibody Dynamic Model for the Vehicle–Line and Determination of Key Parameters

In this section, a multibody dynamics model of vehicle and track interaction is established. The model's complexity is then reduced by performing a sensitivity analysis to discover which parameters have a greater influence on its wheel–rail force output.

2.1. Multibody Dynamics Model of Vehicle and Track Interaction

With the data of a Chinese C80 heavy-haul freight train taken as the primary modeling parameters, as presented in Table 1 [16], a vehicle–line coupling multibody dynamic model was constructed by adopting SIMPACK 2018. The car body is represented using K6 bogie, and the rigid parts such as the wheelset, axle box and frame relate to each other by force elements. The primary spring and the primary vertical shock absorber are constructed from linear force elements and nonlinear viscoelastic force elements, respectively. The wheelset and the frame are linked via the primary suspension system, and the secondary suspension consists of the secondary lateral shock absorber, an anti-yaw shock absorber, etc. The frame and the car body are connected through the secondary suspension system [17,18]. The contact at the interface of the track and wheelset was examined using Hertz contact theory. The wheelset thread is considered as an LMA worn tread, and wheel–track rolling contact modeling was carried out using the FASTSIM algorithm. The track irregularity excitation was calculated using the American Class V track spectrum.

Table 1. Core parameters of the vehicle–track coupled system model.

Dynamical Parameter	Symbol	Initial Value
Wheelset weight/(kg)	X_1	1200
Wheelset rolling moment of inertia (relative to center of mass)/(kg·m^2)	X_2	800
Wheelset pitching moment of inertia (relative to center of mass)/(kg·m^2)	X_3	110
Wheelset yawing moment of inertia (relative to center of mass)/(kg·m$_2$)	X_4	800
Load-bearing saddle weight/(kg)	X_5	27
Load-bearing saddle rolling moment of inertia (relative to center of mass)/(kg·m^2)	X_6	0.4
Load-bearing saddle pitching moment of inertia (relative to center of mass)/(kg·m^2)	X_7	0.2
Load-bearing saddle yawing moment of inertia (relative to center of mass)/(kg·m^2)	X_8	0.4
Longitudinal span of cross rod pin hole/(m)	X_9	1
Horizontal span of cross rod pin hole/(m)	X_{10}	1.981
Lateral span of resilient side bearing/(m)	X_{11}	1.52
Stop clearance/(mm)	X_{12}	12
Primary suspension longitudinal stiffness/(MN·m^{-1})	X_{13}	14
Primary suspension lateral stiffness/(MN·m^{-1})	X_{14}	10
Primary suspension vertical stiffness/(MN·m^{-1})	X_{15}	170
Secondary suspension longitudinal stiffness/(MN·m^{-1})	X_{16}	1.8
Secondary suspension lateral stiffness/(MN·m^{-1})	X_{17}	1.8
Secondary suspension lateral shock absorber damping/(MN·s·m^{-1})	X_{18}	50
Swing arm node longitudinal/vertical stiffness/(MN·m^{-1})	X_{19}	30000
Primary spring longitudinal/lateral stiffness/(MN·m^{-1})	X_{20}	1000

2.2. Determination of Key Parameters of Train-Line Coupling Multibody Dynamic Model

According to relevant experience and expert knowledge, the 10 suspension parameters X_{11}~X_{20} shown in Table 1 have important impacts on the vehicle suspension system [13,19,20]; therefore, they are defined as the main suspension parameters. To simplify the structure of the proxy model, a sensitivity analysis method is further adopted to screen the most critical influencing parameters out of these main suspension parameters. The process is as follows:

(1) Taking wheel–rail force as the optimization target, 1000 samples of each of these 10 suspension parameters were taken randomly using the LHS (Latin hypercube sampling) method [21] within their respective parameter ranges. The specific sampling range is shown in Table 2.

Table 2. Suspension parameter design values.

Dynamical Parameter	Minimum	Maximum
X_{11}	0.76	2.28
X_{12}	6	18
X_{13}	7	21
X_{14}	5	15
X_{15}	85	255
X_{16}	0.9	2.7
X_{17}	0.9	2.7
X_{18}	25	75
X_{19}	15,000	45,000
X_{20}	500	1500

(2) The Sobol global sensitivity analysis method was used [22,23] to assess how input parameters affect the model's output. It can assess the impact of the input dynamical parameters on the variation of wheel–track forces. Based on the values of 10 suspension parameters sampled using the Latin hypercube method and the corresponding forces acting vertically and laterally on the wheels and rails, the global sensitivity coefficients S_t of parameters X11-X20 to wheel–rail forces were calculated, and the sensitivity analysis results are shown in Figure 2.

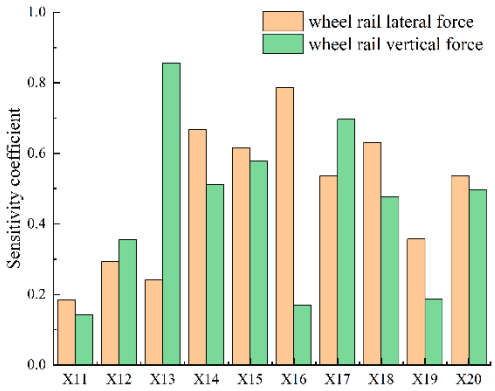

Figure 2. Sensitivity analysis results of dynamical parameters.

The larger the sensitivity coefficient, the greater the influence of the parameter on the target; conversely, the lower the coefficient, the smaller the impact of the parameter on the target. As shown in Figure 2, parameters X_{14}, X_{15}, X_{16} and X_{18} have greater effects on wheel–track lateral interaction force, while X_{13}, X_{15} and X_{17} have a greater effect on wheel–track vertical interaction force. Based on the above results, these six parameters were defined as key suspension parameters.

3. Construction of the CNN-GRU Proxy Model

With the advancement of deep learning technologies, neural network models are widely used in various fields, showing great performance, especially in processing time-series data. As a feedforward neural network, the Convolutional Neural Network [24] is particularly suitable for image recognition and signal processing tasks. It captures the spatial structural characteristics of input data through local connections and weight sharing

mechanisms. CNN can be used to extract spatiotemporal characteristics of the vehicle movement data, for instance, wheel–track interaction forces, acceleration values, and other time-varying patterns of signals. The GRU (gated recurrent unit) [25] is derived from the LSTM network. It has a simplified LSTM structure while maintaining a capacity for handling long-range dependence. The GRU regulates the flow of information by creating update and reset gates, allowing the network to better remember past information and ignore irrelevant information.

In this section, a CNN-GRU hybrid model is proposed, leveraging the feature extraction capabilities of CNN and the strong capacity of GRU for time-series prediction. The hybrid model's purpose is to extract key characteristics from the primitive vehicle movement data using CNN and to construct a time-evolution model for these features through GRU, so that an efficient estimation of suspension parameters can finally be achieved. The proposed model's structure is illustrated in Figure 3.

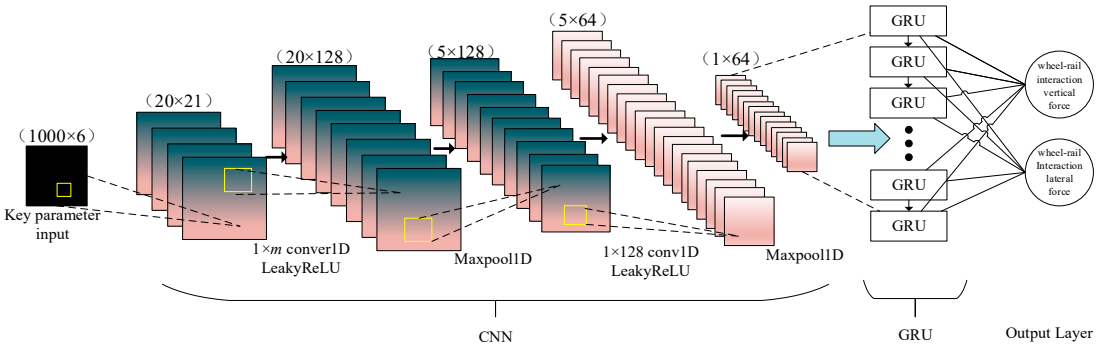

Figure 3. Architecture of the CNN-GRU agent model.

The input of the proxy model is the values screened out by a sensitivity analysis of the six key suspension parameters already defined. Each parameter contains data of 1000 time steps, the data for each time step are collected at three different time points, forming twenty-one features, forming a total of six channels. The outputs of the model are wheel–track lateral interaction force and vertical interaction force. To generate training data, a sliding window was used for sampling, employing a 20 × 21 window and a step increment of one. It generated 980 small fragments arranged in time order, each of which is a 20 × 21 matrix. The overall operation procedure is as follows:

(1) Convolutional layers are mainly used to extract spatial features from input data. A one-dimensional convolution kernel with dimensions [1,1] and a step increment of one was adopted to ensure effective feature extraction. In the first round of convolution, 21 depths were set, with a step size of 1, using the activation function ReLU. The depth of the second round of convolution was increased to 128, and the LeakyReLU activation function was used to capture nonlinear features. Then, down sampling was performed through the max pooling layer with a [2,1] window and a step interval of one. This aids in lowering the number of parameters and extracting key features, while maintaining timing continuity. Via the above processing approach, each small fragment was transformed into feature data with 64 channels. To reduce the likelihood of overfitting, a dropout layer was introduced with a value of 0.2;

(2) To capture the temporal dependencies in these feature data, gated recurrent units were added to the model. The GRU layer is able to analyze the data in both forward and reverse directions, enabling us to more comprehensively mine the contextual information in time-series data. We then adopted a three-layer GRU. The number of hidden units in GRU layer 1 was 64, with the input being feature data processed through convolution and pooling. GRU layer 2 had 32 hidden units, and GRU layer 3 had 16 hidden units. The results from the GRU layer were fed into the fully connected layers. The numbers of elements in the fully connected layers were 64, 8, and

1, respectively, ensuring that the model was able to gradually map high-dimensional features to low-dimensional wheel–track interaction forces;

(3) The forecast output values of wheel–track interaction forces were compared with the simulated values to validate the model's accuracy. The outcomes are depicted in Figure 4.

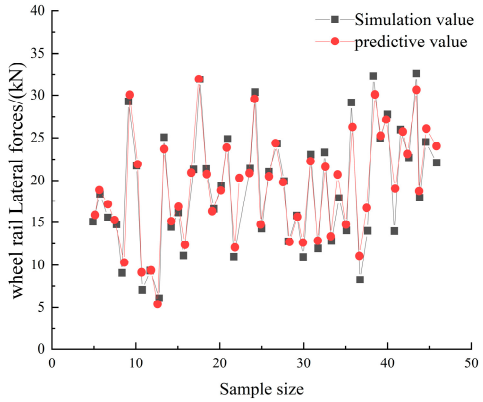

(**a**) wheel–track lateral interaction force

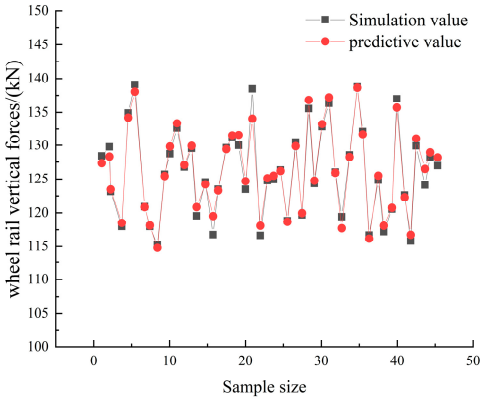

(**b**) wheel–track vertical interaction force

Figure 4. Comparison of SIMPACK simulation values and model prediction values.

4. Dynamic Parameter Estimation Based on Measured Data

In this section, the suspension parameters of C80 heavy-duty freight trains were estimated using NSGA-II, with the help of the above CNN-GRU model and the measured data.

4.1. Introduction of Instrumented Wheelset

The measured wheel–track interaction force data used in this paper were derived from a heavy-freight transportation line in China. Figure 5 demonstrates the instrumented wheelset installed in the heavy-duty freight train. It can facilitate the real-time measurement of the wheel–track interaction force. The force-measuring wheelset can continuously capture key mechanical data during the running of the freight train, providing an important basis for vehicle dynamics analysis and suspension parameter estimation.

Figure 5. Instrumented wheelset detection system.

4.2. NSGA-II Parameter Estimation Based on the Proxy Model

Compared with traditional genetic algorithms, NSGA-II (Non-dominated Sorting Genetic Algorithm II) [26,27] adopts the concepts of fast non-dominated sorting and crowding. This significantly increases the rate at which iterations converge, significantly lowers computational complexity, and guarantees population variety so that the optimal solution set can be found among multiple and conflicting objectives. With certain constraints, NSGA-II can find the best combination of suspension parameters. Its principle is illustrated in Figure 6.

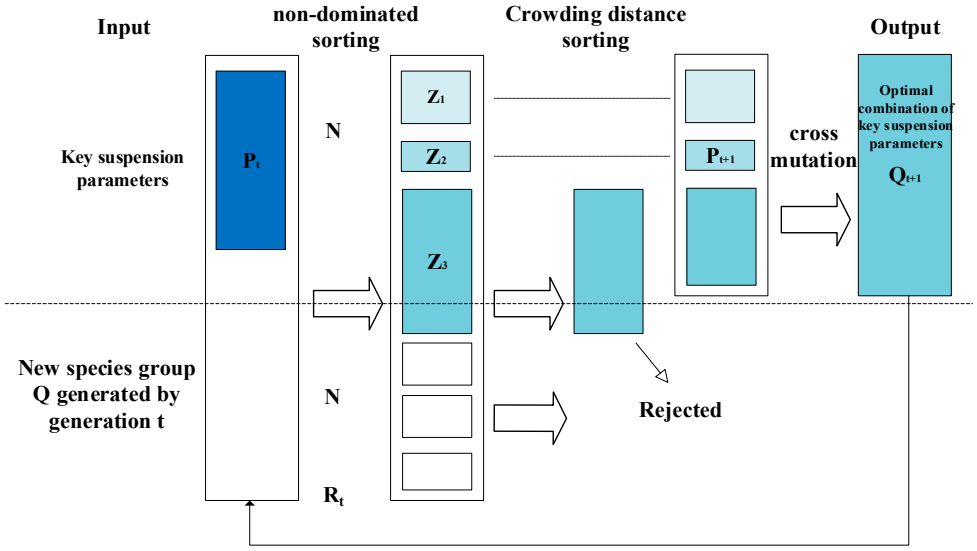

Figure 6. Schematic depiction of the NSGA-II principle.

The core idea of NSGA-II is to perform non-dominant sorting on the population and select excellent individuals for genetic operation according to the sorting results and crowding information. First, an initial population P_t is randomly generated. It contains a certain number of individuals. Each one represents a possible solution consisting of a set of decision variables, ranked in a non-dominated fashion according to the individual's objective function value. The non-dominant hierarchy defines the criteria for one individual to be better than another, i.e., an individual is better than another if it outperforms the other in all goal functions. Through non-dominated sorting, the population can be divided into multiple frontiers (F_1, F_2, F_3,…). For each individual on the frontier, the crowding distance between them is computed. This facilitates the consideration of diversity and distribution when selecting new population members. A new candidate population Q_t is generated through hybridization and mutation operations. The original population and the

newly generated candidate population are then merged. By comparing the non-dominated level and crowding distance of individuals in the two populations, the highest-performing individuals are selected to be part of the next population. The algorithm's flow is illustrated in Figure 7.

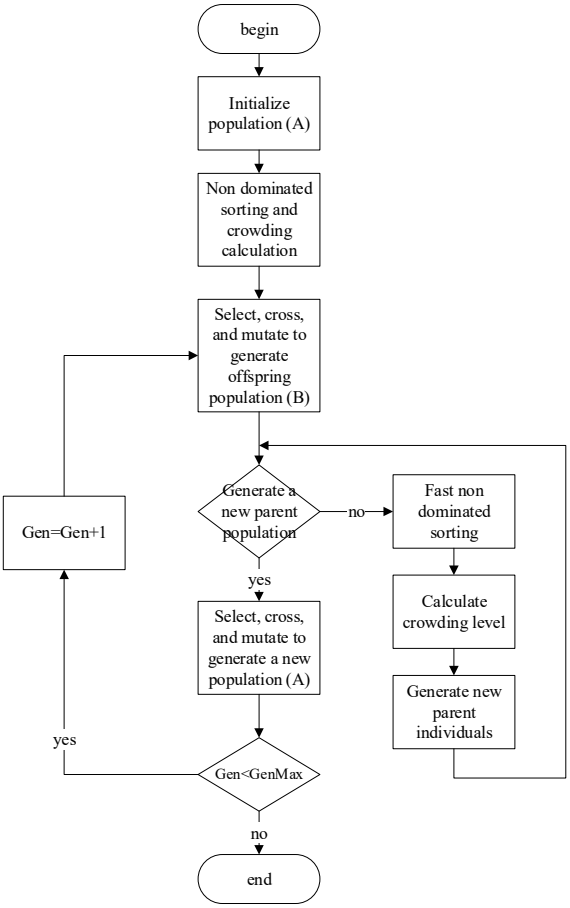

Figure 7. Flow diagram of NSGA-II.

In this section, the main research objective is to minimize the difference between simulated and measured wheel–rail forces. Taking the sensitivity analysis results in Section 2.2 as the design variables, considering that the wheel–rail force includes vertical and lateral forces, the wheel–rail force is divided into two components. The specific objectives are to compare the difference between the predicted wheel–rail lateral force from simulated data and the actual measured wheel–rail lateral force, as well as the difference between the predicted wheel–rail vertical force from simulated data and the actual measured wheel–rail vertical force. The optimization objectives are determined as follows:

$$\min\left\{\left|\hat{y}_i - y_i\right|\right\} \tag{1}$$

The following parameters were used: population size 50, crossover probability 0.9, mutation probability 0.05, and 100 iterations. Figure 8 illustrates the convergence of X_{13}. It is discernible that X_{13} gradually converges to a certain stable value and fluctuates slightly around this value.

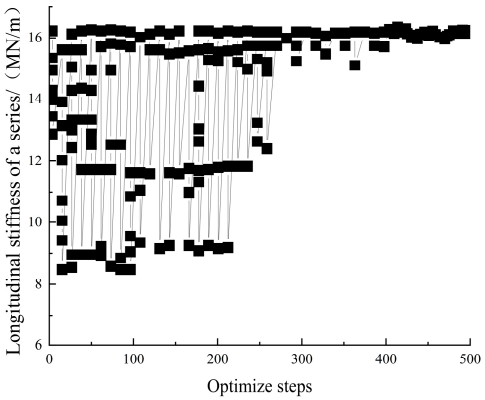

Figure 8. Convergence of primary suspension longitudinal stiffness.

After the optimization calculation, Figure 9 shows the Pareto front of NSGA-II. Tables 3 and 4 provide some information about NSGA-II during operation, where the first column represents the current number of iterations, the second column represents the total number of evaluated individuals, the third column represents the number of non-dominated solutions, the fourth column represents the convergence index, and the fifth column represents the evaluation index. Ideal indicates that the current solution set is close to the ideal solution, f indicates that there is no significant change in the current solution set, and nadir indicates that the current solution set is closest to the worst solution. In the later stage of optimization, a smaller EPS value indicates that the solution set is close to the optimal solution. The indicator is mainly f, indicating that the solution set tends to be stable.

We substituted the corrected results into the vehicle–line coupled multibody dynamics model, and the initial values and estimated results of key dynamic parameters are listed in Table 5.

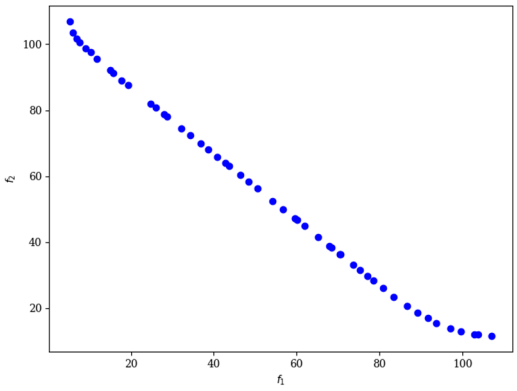

Figure 9. The Pareto frontier of NSGA-II.

Table 3. Middle stage of the algorithm.

n_gen	n_eval	n_nds	eps	Indicator
111	1150	50	0.0381746939	ideal
112	1160	50	0.0006818878	f
113	1170	50	0.0010485927	f
114	1180	50	0.0024256293	f
115	1190	50	0.0034794493	f
116	1200	50	0.0016466931	f
117	1210	50	0.0023378674	f
118	1220	50	0.0073210258	nadir

Table 4. Late stage of the algorithm.

n_gen	n_eval	n_nds	eps	Indicator
493	4970	50	0.0028696928	f
494	4980	50	0.0005592864	f
495	4990	50	0.0018608608	f
496	5000	50	0.0033501854	f
497	5010	50	0.0003631807	f
498	5020	50	0.0010969726	f
499	5030	50	0.0016310799	f
500	5040	50	0.0018601757	f

Table 5. Key settings' estimation outcome.

Dynamic Parameter	Initial Value	Estimated Value
X_{13}	14	16.1
X_{14}	10	8.3
X_{15}	170	164
X_{16}	1.8	1.7
X_{17}	1.8	1.91
X_{18}	50	51.3

5. Experiment Result Analysis

This section describes the experiment and its outcomes in depth. Considering the complexity of each working condition, only three working circumstances, i.e., straight line, curved line, and long and steep uphill, were considered for the wheel–track interaction force in the current work. The specific parameter settings of each working condition are shown in Table 6, while different settings of the same working condition type were not considered here.

Table 6. Parameter settings of three typical working conditions.

Working Condition	Speed	Curve Radius	Slope
Straight line	60 km/h		
Curved line	60 km/h	300 m	
Long and steep uphill line	60 km/h		0.1

5.1. Performance Comparison of Several Models

To better illustrate the efficacy of the method presented in this research, the CNN-GRU model is assessed alongside the RBF, CNN-LSTM, BP and CNN-BiLSTM models [28–30], as shown in Figures 10 and 11. To more intuitively display the model's forecast accuracy, the relative error was employed to assess the discrepancy between predicted and simulated values. The results are given in Table 7. The formula is as follows [31,32]:

$$\left|\frac{\Delta x}{x}\right| = \left|\frac{y - y_i}{y_i}\right| \quad (2)$$

where y represents the value predicted by various models, and y_i represents the value simulated by the vehicle–line coupling multibody dynamic model.

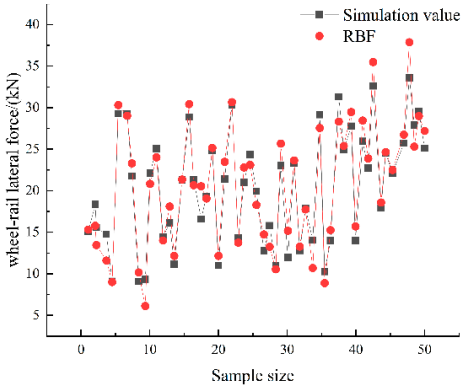

(**a**) RBFNN

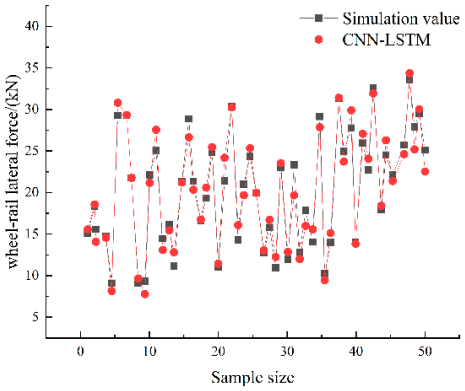

(**b**) CNN-LSTM

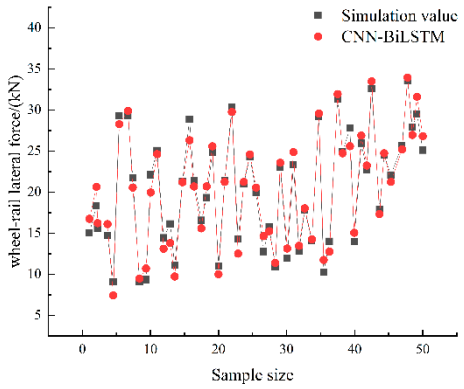

(**c**) CNN-BiLSTM

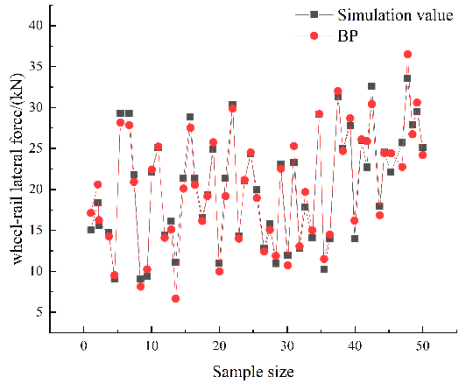

(**d**) BP

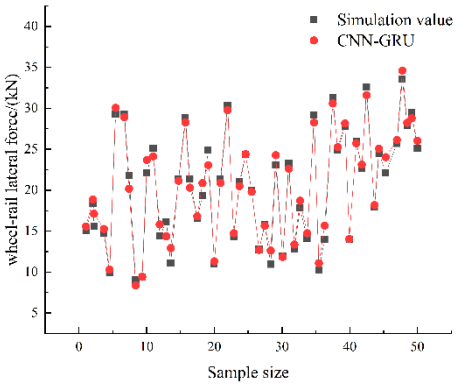

(**e**) CNN-GRU

Figure 10. Comparison of predicted and simulated values of wheel–track lateral interaction force by different combinations of models and algorithms.

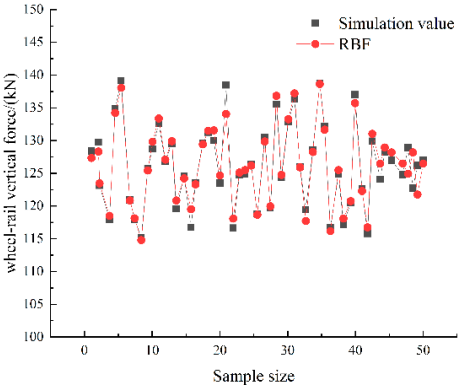

(**a**) RBFNN

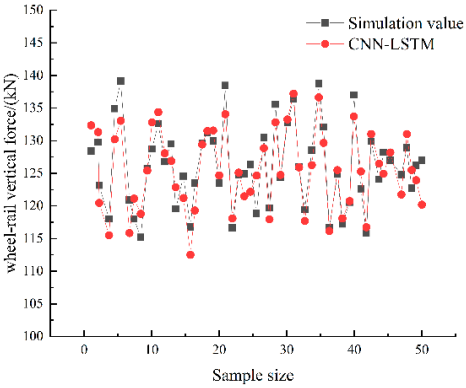

(**b**) CNN-LSTM

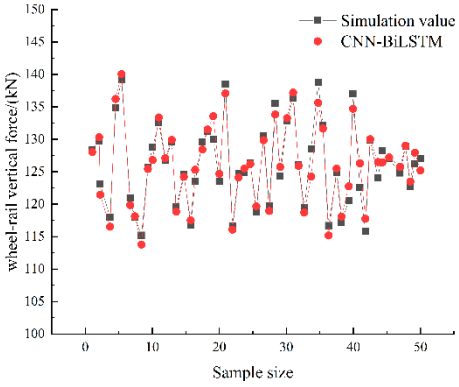

(**c**) CNN-BiLSTM

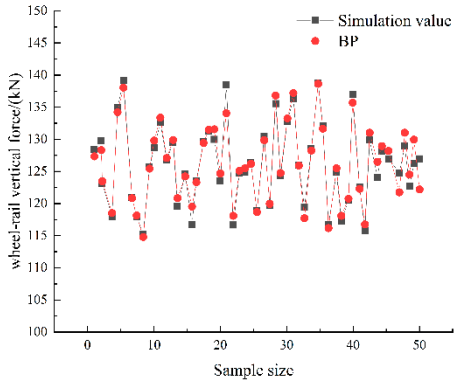

(**d**) BP

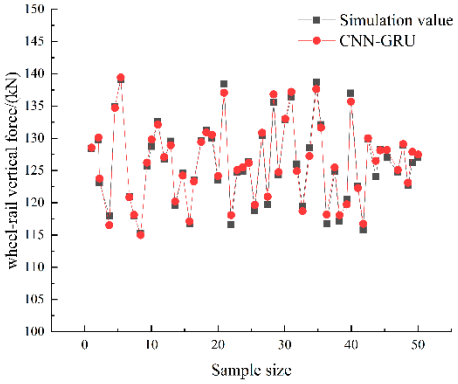

(**e**) CNN-GRU

Figure 11. Comparison of predicted and simulated values of wheel–track vertical interaction force by integrating various models and algorithms.

Table 7. Relative error of wheel–rail forces by integrating various models and algorithms.

	Simulated Wheel–Rail Vertical Force/(kN)	Predicted Value	Relative Error Rate	Simulated Wheel–Rail Lateral Force/(kN)	Predicted Value	Relative Error Rate
RBF	126.13	123.86	1.80%	20.3	22.35	10.09%
CNN-LSTM	126.13	123.91	1.76%	20.3	21.73	7.04%
CNN-BiLSTM	126.13	128.38	1.78%	20.3	21.24	4.63%
BP	126.13	129.04	2.30%	20.3	18.97	6.55%
CNN-GRU proposed in this paper	126.13	128.13	1.56%	20.3	19.57	3.59%

As shown above, for wheel–track lateral interaction force, the RBF model has the highest relative error rate of 10.09%, whereas this value in the other models is relatively low, and the method proposed in this research has the lowest relative error ratio of 3.59%. For the values of wheel–track vertical interaction force, the numerical fluctuation is small, and the relative error rate of incidence of the proposed method is minimal, at 1.56%. In other words, the CNN-GRU model described in this paper can provide better forecasting accuracy.

5.2. Comparison of Wheel–Rail Forces Before and After Parameter Estimation

The parameter estimation results in Section 4.2 were introduced into the train–line coupling multibody dynamic model based on C80 data, and the simulated forces were compared with the forces measured by the instrumented wheelset, before and after using the estimated parameters. The wheel–rail lateral force results produced under three working conditions before and after parameter correction are shown in Figures 12 and 13.

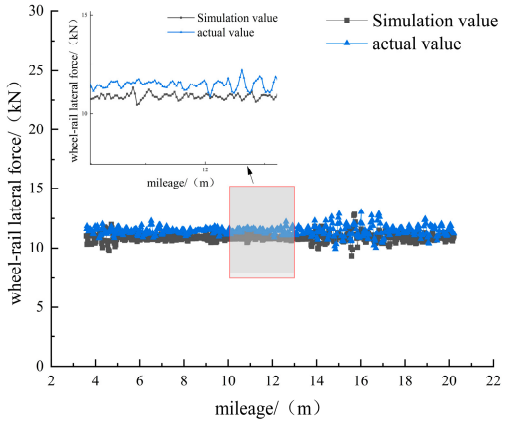

(**a**) Straight line

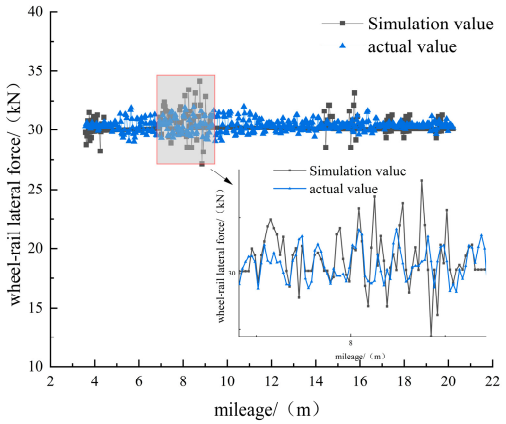

(**b**) Curved line

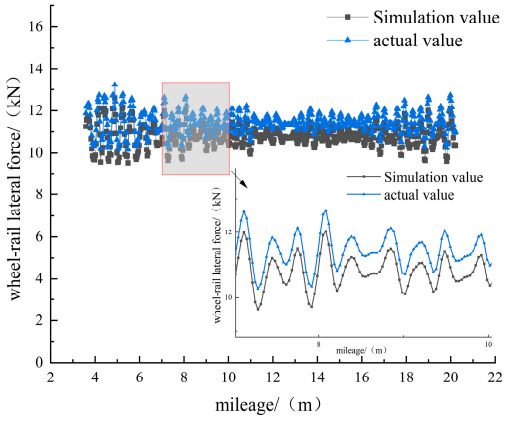

(**c**) Long and steep uphill line

Figure 12. Comparison of simulated and measured values of wheel–track lateral interaction force before and after using the estimated parameters.

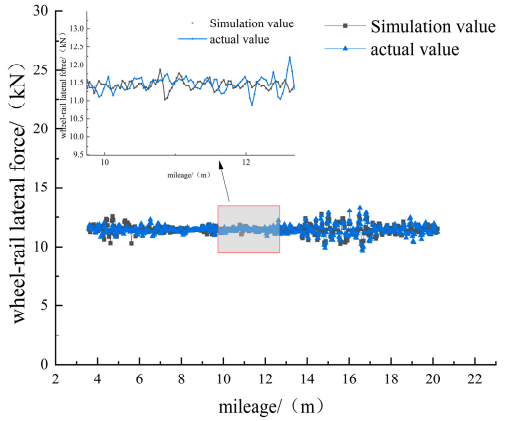

(**a**) Straight line

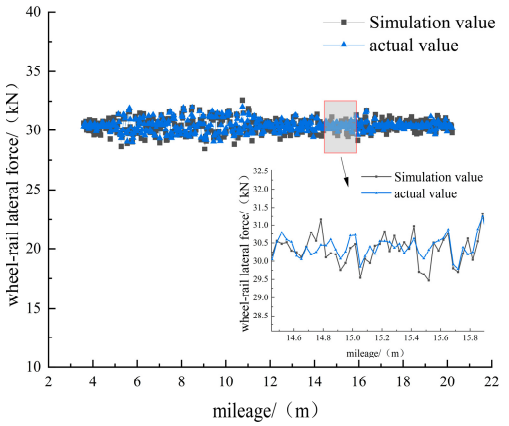

(**b**) Curved line

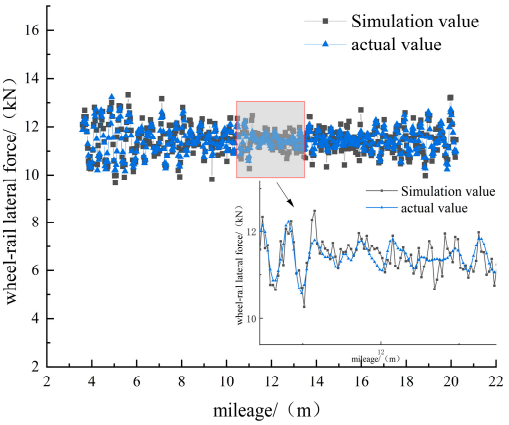

(**c**) Long and steep uphill line

Figure 13. Comparison of simulated and real-world values of wheel–track lateral interaction force after using the estimated parameters.

The simulated values of wheel–track lateral interaction force before and after using the estimated suspension parameters were compared separately with the measured force values, and relative error was used to evaluate the accuracy before and after the parameter correction. Tables 8 and 9 present the results of the comparison between the simulated and real-world values of wheel–track lateral interaction force before and after parameter correction.

Table 8. Comparison of simulated and real-world values of wheel–track interaction force before parameter correction.

Working Condition	Simulated Wheel–Rail Lateral Force/(kN)	Measured Wheel–Track Force	Error Rate	Simulated Wheel–Track Vertical Interaction Force/(kN)	Measured Wheel–Track Interaction	Error Rate
Straight line	12.48	11.42	9.28%	140.20	138.91	0.93%
Curved line	31.52	29.67	6.24%	131.28	128.12	2.47%
Long and steep uphill line	13.24	11.21	18.11%	140.95	138.17	2.01%

Table 9. Comparison of simulated and real-world values of wheel–track interaction force after parameter correction.

Working Condition	Simulated Wheel–Rail Lateral Force/(kN)	Measured Wheel–Track Force	Error Rate	Simulated Wheel–Track Vertical Interaction Force/(kN)	Measured Wheel–Track Interaction	Error Rate
Straight line	12.22	11.42	7.00%	140.54	138.91	1.17%
Curved line	31.01	29.67	4.52%	130.71	128.12	2.02%
Long and steep uphill line	12.38	11.21	10.44%	139.34	138.17	0.85%

The statistics in Tables 8 and 9 show that, under different working conditions, the error produced in simulating wheel–rail force is significantly improved after using the estimated suspension parameters, i.e., after the suspension parameters are corrected. Specifically, the error rate of the wheel–track lateral interaction force decreases from 9.28% to 7.00%, while the error of wheel–track vertical interaction force increases slightly from 0.93% to 1.17% under the straight-line condition. Under the curved-line condition, the error rate of wheel–track lateral interaction force decreases from 6.24% to 4.52%, and from 2.47% to 2.02% for the vertical force. Under the long and steep uphill conditions, the error rate of wheel–track lateral interaction force decreases greatly from 18.11% to 10.44%, and from 2.01% to 0.85% for the wheel–track vertical interaction force. These results show that the error between the simulated and real-world values of the wheel–track interaction force is significantly reduced by suspension parameter correction, especially under complex working conditions (such as curved line and long and steep uphill line). This fully demonstrates the efficacy of the strategy provided in this study in improving the accuracy of the simulation model and the operational safety of the train.

6. Conclusions

This paper aimed to achieve accurate estimation of the suspension parameters for heavy-duty freight trains by building a CNN-GRU proxy model combined with a sensitivity analysis and an optimization algorithm, and herein, we have conducted comparative experiments before and after using the estimated suspension parameters. The significant results are as follows:

(1) For the C80 freight train, under the three typical working conditions mentioned in this paper, the primary suspension longitudinal stiffness, the secondary suspension vertical stiffness, and the secondary suspension lateral stiffness have stronger effects on the wheel–track vertical interaction force, while the primary lateral stiffness, primary vertical stiffness, secondary lateral shock absorber damping, and secondary longitudinal stiffness have greater effects on the wheel–track lateral interaction force;

(2) Through comparative experiments, the effectiveness of the suggested CNN-GRU proxy model has been verified. The investigation results reveal that by using the optimized suspension parameters, the accuracy of the multibody dynamics simulation model was significantly elevated, and the peak value of the wheel–rail force was reduced, such that the risk of derailment was reduced, and the operational safety and stability of heavy-haul freight trains were effectively improved;

(3) The NSGA-II algorithm based on the CNN-GRU model proposed in this work demonstrates remarkable effectiveness in the estimation of suspension parameters for heavy-duty freight trains. This method can more accurately identify changes in suspension parameters. It provides a new approach to augmenting the safety and stability of train operation.

The method proposed in this study is suitable for estimating the suspension parameters of C80 heavy-duty trucks. In future research, the generalizability of this method when using different vehicle types and operating conditions can be further explored so as to extend it to other types of transportation systems. By combining advanced machine learning technology and visual inspection methods, the real-time monitoring and dynamic adjustment of vehicle status can be realized to further improve the safety and efficiency of transportation systems. Future research can be devoted to exploring more complex conditions, a wider variety of suspension parameters, and how to apply these technologies to online monitoring and fault diagnosis systems used in actual operations so as to achieve more intelligent and automated transportation management.

Author Contributions: C.Z., conceptualization, methodology. Y.W., data analysis and writing. J.H., validation, English writing and providing guidance on the revision process. All authors have read and agreed to the published version of the manuscript.

Funding: This work is supported by the National Key R and D Program of China (2021YFF0501101), National Natural Science Foundation of China (62173137), and the Project of Hunan Provincial Department of Education (23A0426).

Data Availability Statement: The data presented in this study are available on request from the corresponding author since the data in this study come from a national key project.

Conflicts of Interest: The authors declare no conflicts of interest.

References

1. Cao, Y.; Liu, Y.; Sun, Y.; Su, S.; Wang, F. Enhancing rail safety through real-time defect detection: A novel lightweight network approach. *Accid. Anal. Prev.* **2024**, *203*, 107617.
2. He, J.; Xiao, Z.; Zhang, C. Predicting the remaining useful life of rails based on improved deep spiking residual neural network. *Process Saf. Environ. Prot.* **2024**, *188*, 1106–1117.
3. Alrejjal, A.; Ksaibati, K. Impact of mountainous interstate alignments and truck configurations on rollover propensity. *J. Saf. Res.* **2022**, *80*, 160–174.
4. Corrêa, P.; Ramos, P.; Teixeira, L.; dos Santos, G.; dos Santos, A. Dynamic simulation of a heavy-haul freight car under abnormal braking application on tangent and curve. *Veh. Syst. Dyn.* **2023**, *61*, 2456–2471.
5. Wang, Q.; Jiang, X.; Zeng, J.; Mao, R.; Wei, L.; Wu, S. Innovative method for high-speed railway carbody vibration control caused by hunting instability using underframe suspended equipment. *J. Vib. Control* **2024**, 10775463241272954. https://doi.org/10.1177/10775463241272954
6. Zhang, H.; Ling, L.; Zhai, W. Adaptive nonlinear damping control of active secondary suspension for hunting stability of high-speed trains. *Appl. Math. Model.* **2024**, *133*, 79–107.
7. Liu, J.; Du, D.; He, J.; Zhang, C. Prediction of Remaining Useful Life of Railway Tracks based on DMGDCC-GRU Hybrid Model and Transfer Learning. *IEEE Trans. Veh. Technol.* **2024**, *73*, 7561–7575.
8. Xu, Z.; Saleh, J.H. Machine learning for reliability engineering and safety applications: Review of current status and future opportunities. *Reliab. Eng. Syst. Saf.* **2021**, *211*, 107530.
9. Yang, H.; He, J.; Liu, Z.; Zhang, C. LLD-MFCOS: A Multi-scale Anchor-Free Detector Based on Label Localization Distillation for Wheelset Tread Defect Detection. *IEEE Trans. Instrum. Meas.* **2023**, *73*, 1–15.
10. He, Y.; Yu, H.; Yang, Z.; Sun, W.; Feng, M.; Mian, A. Danet: Density adaptive convolutional network with interactive attention for 3d point clouds. *IEEE Robot. Autom. Lett.* **2023**, *8*, 5496–5503.
11. Wang, J.; Yu, H.; Lin, X.; Li, Z.; Sun, W.; Akhtar, N. EFRNet-VL: An end-to-end feature refinement network for monocular visual localization in dynamic environments. *Expert Syst. Appl.* **2024**, *243*, 122755.
12. Issa, M.; Samn, A. Passive vehicle suspension system optimization using Harris Hawk Optimization algorithm. *Math. Comput. Simul.* **2022**, *191*, 328–345.
13. He, Q.; Li, L.; Li, C.; Wang, P.; Xie, S. Approximate Bayesian Estimation of Suspension Parameters of In-service High-speed Trains Based on Kriging Surrogate Model. *J. Mech. Eng.* **2023**, *59*, 139–148.
14. Zou, H.; Wu, Q.; Zou, X. Research on optimization design of suspension parameters of railway vehicle bogies based on surrogate model. *Multimed. Tools Appl.* **2022**, 1–19. https://doi.org/10.1007/s11042-022-14022-4

15. Pan, Y.; Sun, Y.; Li, Z.; Gardoni, P. Machine learning approaches to estimate suspension parameters for performance degradation assessment using accurate dynamic simulations. *Reliab. Eng. Syst. Saf.* **2023**, *230*, 108950.
16. Zhou, S. *SIMPACK 9 Example Tutorial*; Beijing United Publishing Company: Beijing, China, 2013.
17. Llopis-Albert, C.; Rubio, F.; Zeng, S. Multiobjective optimization framework for designing a vehicle suspension system. A comparison of optimization algorithms. *Adv. Eng. Softw.* **2023**, *176*, 103375.
18. Zhang, H.; Ling, L.; Zhang, Z.; Zhai, W. Robust Constraint-Following Control for Bio-Inspired Structure Oriented Active Suspension System of High-Speed Trains. *IEEE Trans. Intell. Transp. Syst.* **2024**, *25*, 16107–16117.
19. Jian-ping, Z.; Ji-ye, Z.; Tian, L. Multi-objective optimization for dynamics parameters of high-speed trains under side wind. *J. Traffic Transp. Eng.* **2020**, *20*, 80–88.
20. Ye, Y.; Huang, P.; Zhang, Y. Deep learning-based fault diagnostic network of high-speed train secondary suspension systems for immunity to track irregularities and wheel wear. *Railw. Eng. Sci.* **2022**, *30*, 96–116.
21. Zhong, R.; Yu, J.; Zhang, C.; Munetomo, M. SRIME: A strengthened RIME with Latin hypercube sampling and embedded distance-based selection for engineering optimization problems. *Neural Comput. Appl.* **2024**, *36*, 6721–6740.
22. Chauhan, M.S.; Ojeda-Tuz, M.; Catarelli, R.A.; Gurley, K.R.; Tsapetis, D.; Shields, M.D. On active learning for Gaussian process-based global sensitivity analysis. *Reliab. Eng. Syst. Saf.* **2024**, *245*, 109945.
23. Tansar, H.; Duan, H.-F.; Mark, O. Global sensitivity analysis of bioretention cell design for stormwater system: A comparison of VARS framework and Sobol method. *J. Hydrol.* **2023**, *617*, 128895.
24. Oyedeji, O.A.; Khan, S.; Erkoyuncu, J.A. Application of CNN for multiple phase corrosion identification and region detection. *Appl. Soft Comput.* **2024**, *164*, 112008.
25. Zulqarnain, M.; Ghazali, R.; Aamir, M.; Hassim, Y.M.M. An efficient two-state GRU based on feature attention mechanism for sentiment analysis. *Multimed. Tools Appl.* **2024**, *83*, 3085–3110.
26. Ma, H.; Zhang, Y.; Sun, S.; Liu, T.; Shan, Y. A comprehensive survey on NSGA-II for multi-objective optimization and applications. *Artif. Intell. Rev.* **2023**, *56*, 15217–15270.
27. Zahmatkesh, S.; Karimian, M.; Chen, Z.; Ni, B.-J. Combination of coagulation and adsorption technologies for advanced wastewater treatment for potable water reuse: By ANN, NSGA-II, and RSM. *J. Environ. Manag.* **2024**, *349*, 119429.
28. Dao, F.; Zeng, Y.; Qian, J. Fault diagnosis of hydro-turbine via the incorporation of bayesian algorithm optimized CNN-LSTM neural network. *Energy* **2024**, *290*, 130326.
29. Li, G.; Ma, S.; Zhang, D.; Yang, L.; Zhang, W.; Wu, Z. An efficient sequential anisotropic RBF reliability analysis method with fast cross-validation and parallelizability. *Reliab. Eng. Syst. Saf.* **2024**, *241*, 109600.
30. Song, B.; Liu, Y.; Fang, J.; Liu, W.; Zhong, M.; Liu, X. An optimized CNN-BiLSTM network for bearing fault diagnosis under multiple working conditions with limited training samples. *Neurocomputing* **2024**, *574*, 127284.
31. Audrito, A.; Gárriz, A.; Quirós, F. Convergence in relative error for the porous medium equation in a tube. *Ann. Di Mat. Pura Ed Appl.* **2024**, *203*, 149–171.
32. Wang, N.; Liu, Y.; Wang, Z.; Wei, Z.; Tang, R.; Tang, P.; Yu, G. Locally differentially private frequency distribution estimation with relative error optimization. *Front. Comput. Sci.* **2024**, *18*, 185613.